63-3-6

406 688

Quarterly Progress Report

Q-B2089-1

PREPARATION AND EVALUATION OF HIGH PURITY BERYLLIUM

by

G. E. Spangler
M. Herman
E. J. Arndt
D. B. Hoover
V. V. Damiano
C. H. Lee

January 15, 1963 to April 14, 1963

Prepared for

DEPARTMENT OF THE NAVY
Bureau of Naval Weapons

Contract No. NOw 62-0536-d

THE FRANKLIN INSTITUTE
LABORATORIES FOR RESEARCH AND DEVELOPMENT
PHILADELPHIA PENNSYLVANIA

THE FRANKLIN INSTITUTE • *Laboratories for Research and Development*

Quarterly Progress Report Q-B2089-1

PREPARATION AND EVALUATION OF HIGH PURITY BERYLLIUM

by

G. E. Spangler
M. Herman
E. J. Arndt
D. B. Hoover
V. V. Damiano
C. H. Lee

January 15, 1963 to April 14, 1963

Prepared for

DEPARTMENT OF THE NAVY
Bureau of Naval Weapons

Contract No. NOw 62-0536-d

TABLE OF CONTENTS

LIST OF FIGURES

LIST OF FIGURES (cont.)

1. INTRODUCTION

The purpose of this investigation is to produce high purity beryllium and to study its deformation and fracture characteristics.

2. ZONE REFINING

2.1 Zone Melting

During the past quarter, the zone melting of another one inch diameter SR grade Pechiney beryllium (vacuum cast and extruded) bar was completed. This bar, the third one inch diameter bar of this particular grade starting material, was subjected to a total of ten zone passes at a rate of one half inch per hour.

Four zone passes at this same rate were also made through a one quarter inch diameter SR grade Pechiney (vacuum cast and extruded) bar.

A second 5 w/o Cu-Be alloy bar was made by melting the appropriate amount of high purity copper wire (wound on the surface of the beryllium bar) into a seven pass SR grade Pechiney (hot extruded flake) bar. This bar was previously seeded to orient the c-axis of the crystal 90° to the bar axis. An additional zone pass was made after the melt-in to attempt to zone level the copper concentration along the length of the bar.

2.2 Automating Device

Some effort has been devoted recently to the development of a scheme for automating the floating zone melting process. This has been done in order to decrease the tediousness and the expense associated with this operation, which at present requires constant visual observation and manual power control. It is also hoped that by automating the process an improvement can be made in the effectiveness of the zone purification. The latter effect can be achieved if fluctuations in the zone interface motion can be minimized through improved control of the length of the molten zone.

The first step in automating the floating zone melting process is the development of a means for accurately sensing the length of the molten zone. Since the zone interface itself is in many cases very difficult to detect even by eye, the best chance of control lies in maintaining a constant temperature at some point within the molten zone. Presumably this could be done by means of a sufficiently sensitive optical pyrometer device. In the zone melting apparatus of the type used for the highly reactive metals, however, it is quite difficult to sight directly at the molten zone. The reason for this is that considerable vapor deposition occurs on the glass protection tube in the vicinity of the molten zone. An alternative approach then, is to control the length of the molten zone by holding constant the temperature of the bar at some fixed position a short distance below the induction coil. While this technique eliminates the need for sighting through a region of vapor deposition, the optical sensing device employed must now be sufficiently sensitive to minimize any delay in its response to changes in temperature of the molten zone.

It has been demonstrated recently in our laboratories that a device using a CdSe photoconductive cell does have sufficient sensitivity for this purpose. By placing the photoconductive cell in one leg of a standard DC bridge circuit, any changes in the amount of light falling on the cell are reflected in the output potential of the bridge circuit. This potential can be readily monitored by standard potentiometric or galvanometric instruments. The photoconducting cell is mounted in an opaque bakelite collimating tube which can be positioned to sight on the bar being zone melted, at some fixed position below the induction coil. By maintaining a constant temperature at this point, the location of the zone interface is fixed with respect to the induction coil and the length of the molten zone will remain constant.

It is understood, of course, that this relation between the molten interface and the control position will be affected by changes in heat flow conditions. These changes will occur at the ends of the bar and in regions were appreciable changes in cross section are p[illegible]. Both the latter effects, however, are relatively long range in nature because of the slow travel rates used for zone melting. As a result, these changes can be compensated for by making gradual adjustments in the temperature of the control position. It is of significance, however, that all present tests indicate that the sensing device is far superior to visual control in reducing the more undesirable short range fluctuations of zone length. The ease of operation has also been greatly increased by permitting the operator to observe changes on a greatly expanded scale on an indicating meter rather than by intently studying the molten zone itself.

At the present time, several schemes are being considered for utilizing the output of the DC bridge circuit as a direct feed-back control for the output of the induction unit. This, of course, is the next step in achieving full or at least semi-automation of the floating melting process. The progress of this next phase of development will be reported in subsequent reports.

3. SINGLE CRYSTAL STUDIES

A room temperature tensile test was performed on a single crystal tensile specimen (CuBe-2-1) from the 5 w/o Cu-Be alloy. The test was performed to determine the critical resolved shear stress for prism slip in this alloy. The specimen was prepared by a combination of electro-spark discharge and electro-chemical machining. The c-axis of the crystal was within 1° of being perpendicular to the tensile axis. The results of the test are as follows:

Crystal CuBe-2-1

CRSS $(10\bar{1}0)$	11,300 PSI	$\chi_o = 31°$
Elongation	56.6%	$\lambda_o = 51$
Shear Strain	72.5%	
Resolved shear stress at fracture $(10\bar{1}0)$	24,500 PSI	

The crystal deformed entirely by duplex glide and exhibited a knife edge fracture.

The increase in the critical resolved shear stress for prism glide resulting from the addition of 5 w/o copper, is much less marked than the corresponding increase observed for basal glide; (from 9000 psi to 11,300 psi for prism glide; from 400 psi to 7800 psi for basal glide).[1] These present results further emphasize the relative insensitivity of prism glide to impurity content.

4. POLYCRYSTALLINE STUDIES

This section describes the swaging of beryllium at five different temperatures, from 425°C to 250°C. In all cases, the starting material was a cylindrical single crystal, one quarter inch in diameter, one and one eighth inch long. These crystals were sectioned from a one inch diameter, eleven pass SR Pechiney bar (1" SR-1). The crystals were all encased in Armco iron jackets and reduced ~ 10% per pass to a final reduction of about 90%, following the hot swaging technique previously described[1].

The annealing procedure was different in some instances. S-5, swaged at 425°C, was annealed three times at 800°C after the second, fourth and sixth passes. S-6, S-7, and S-8 were annealed three times at 650°C in the same sequence described for S-5. S-9 was annealed once at 800°C after the fourth pass. Each of the crystals received a total of 16 to 18 passes. The as-swaged structure of S-5, Figures 1 and 2 appears to

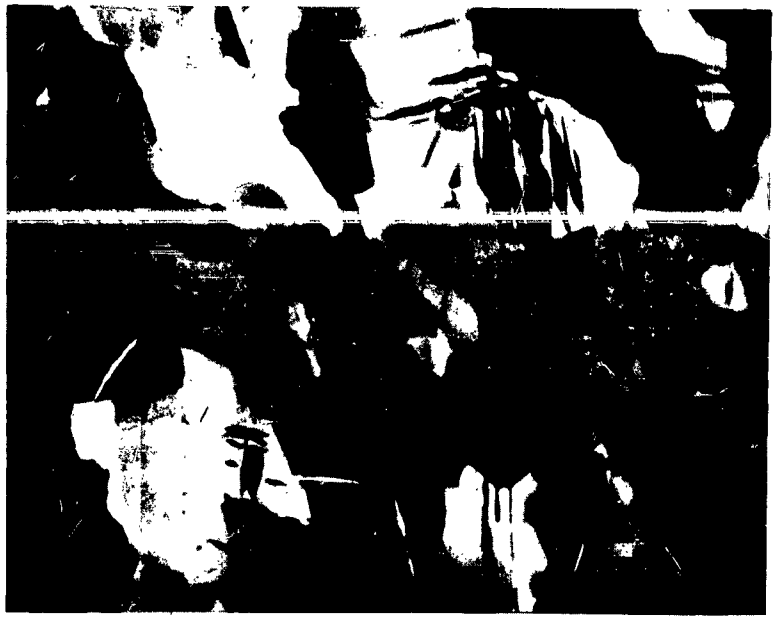

FIG. 2. AS-SWAGED STRUCTURE OF S-2 SWAGED AT 425°C. LONGITUDINAL SECTION. POLARIZED LIGHT, 100X.

FIG. 1. AS-SWAGED STRUCTURE OF S-5, SWAGED AT 425°C. TRANSVERSE SECTION. POLARIZED LIGHT, 100X.

be that of a large grained, polycrystalline aggregate. The grain boundaries are wavy and indistinct. The grains themselves are only moderately twinned, considering that 70-80% reductions followed the last anneal. An interesting aspect to this particular bar is that the longitudinal section differs only slightly from the transverse section. The lack of grain elongation and the moderate twin density indicate that, during the swaging operation, some form of recrystallization has occurred at temperatures well below that at which recrystallization would occur statically.

Some annealing experiments were performed on the as-swaged bar. The annealing was performed in vacuum at pressures $\sim 10^{-6}$ mm Hg. Figure 3 is the longitudinal section of a specimen annealed for 30 minutes at a temperature of 500°C. The main difference between this structure and the as-swaged structure is the absence of twins. The grain boundaries are still wavy and the grain size not markedly changed. When annealed at 400°C for 30 minutes, the structure appeared nearly identical to that of the as-swaged condition.

Figure 4 is a micrograph of a specimen annealed for 15 minutes at 750°C. The grains are now distinct, the grain boundaries straight. This specimen has all the aspects of a completely recrystallized structure. It should be noted, however, that throughout this annealing series there was no definite evidence of nucleation. Initially, the twins annealed out of the structure, followed, at the higher temperatures, by grain boundary migration.

The bar designated S-6 was swaged at 375°C to attempt to refine the as-swaged structure, so that after annealing a fine grained structure could be produced. Figure 5 is a micrograph of the transverse section of S-6. The structure is a refined version of that found in S-5. Figure 6 is a micrograph of the longitudinal section. It appears to have a larger grain size than the transverse section. Annealing

FIG. 4. S-5 ANNEALED AT 750°C FOR 15 MINUTES. LONGITUDINAL SECTION. POLARIZED LIGHT, 100X.

FIG. 3. S-5 ANNEALED AT 500°C FOR 30 MINUTES. LONGITUDINAL SECTION. POLARIZED LIGHT, 100X.

FIG. 6. AS-SWAGED STRUCTURE OF S-6, SWAGED AT 375°C. LONGITUDINAL SECTION. POLARIZED LIGHT, 100X.

FIG. 5. AS-SWAGED STRUCTURE OF S-6, SWAGED AT 375°C. TRANSVERSE SECTION. POLARIZED LIGHT, 100X.

experiments performed on this bar also proved disappointing, so that no micrographs are shown.

Bend tests at room temperature were made on the S-6 wire in the as-swaged condition and after annealing at 750° for 15 minutes. The as-swaged wire was quite brittle. The annealed wire underwent only slight bending prior to fracture.

S-7 was swaged at 300°C. The structure of the transverse section is seen in Figure 7. This micrograph reveals areas of very fine grained structure and areas of larger grains containing twins. The longitudinal section, Figure 8, shows some stringiness but maintains the general appearance of the transverse section. This micrograph is evidence that there is perhaps an additional stage of recrystallization taking place during swaging, producing extremely small and apparently untwinned grains.

Annealing experiments performed on S-7 showed promising results. Figure 9 is a micrograph of a longitudinal section of S-7 annealed at 700°C for 20 minutes. This structure has the appearance of a well annealed polycrystalline aggregate, although it does appear that the grains are strung out along the swaging direction.

The results on S-8 and S-9 may be considered together. S-8 was swaged at 250°C, and S-9 at 275°C. Both specimens were cracked longitudinally. Figure 10 is a micrograph of the transverse section of S-8. The structure is completely fine grained and untwinned. Figure 11 is a micrograph of the longitudinal section of S-8. There is some stringiness along the swaging direction, but the grains are small.

Figure 12 is a transverse micrograph of S-9. The 25°C elevation of the swaging temperature is evidenced in the isolated areas of coarser, twinned grains.

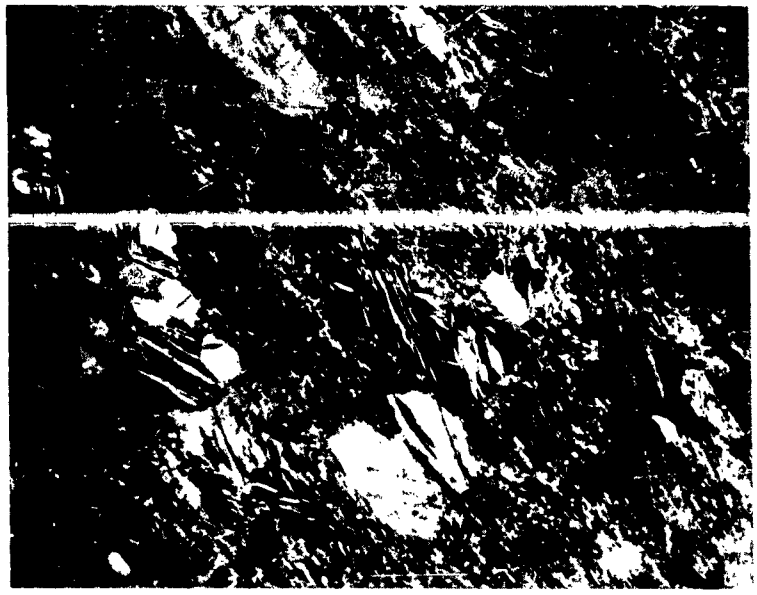

FIG. 8. AS-SWAGED STRUCTURE OF S-7, SWAGED AT 300°C. LONGITUDINAL SECTION. POLARIZED LIGHT, 100X.

FIG. 7. AS-SWAGED STRUCTURE OF S-7, SWAGED AT 300°C. TRANSVERSE SECTION. POLARIZED LIGHT, 100X.

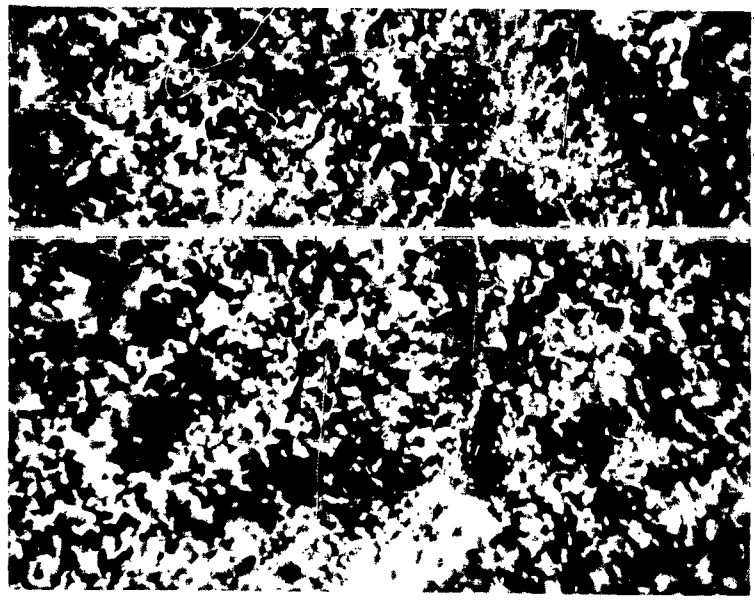

FIG. 10. AS-SWAGED STRUCTURE OF S-8, SWAGED AT 250°C. TRANSVERSE SECTION. POLARIZED LIGHT, 300X.

FIG. 9. S-7 ANNEALED AT 700°C FOR 20 MINUTES. LONGITUDINAL SECTION. POLARIZED LIGHT, 100X.

FIG.12. AS-SWAGED STRUCTURE OF S-7, SWAGED AT 275°C. TRANSVERSE SECTION. POLARIZED LIGHT, 300X.

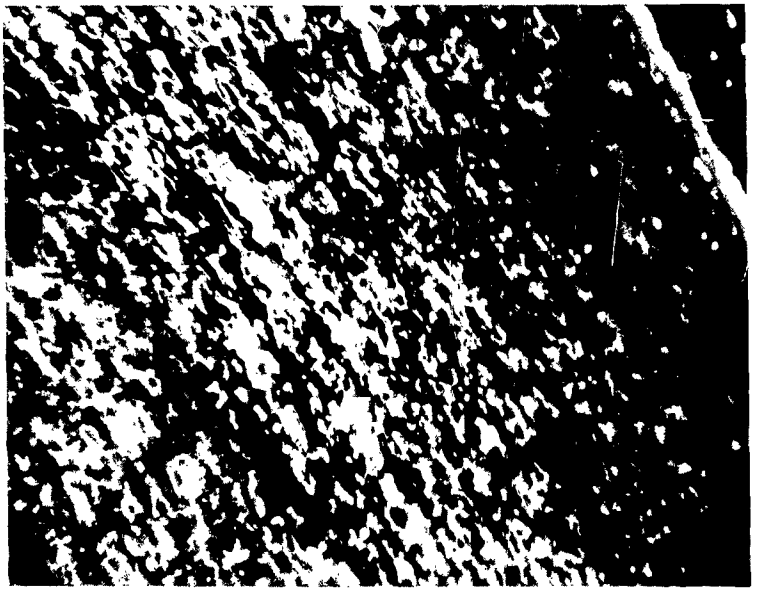

FIG.11. AS-SWAGED STRUCTURE OF S-8, SWAGED AT 250°C. LONGITUDINAL SECTION. POLARIZED LIGHT, 300X.

In all cases investigated here, at swaging temperatures from 425°C to 250°C, it appears that at least one form of dynamic recrystallization is occurring, during which some twins are eliminated and new grains are formed. Decreasing the temperature decreases the equilibrium "grain size" and the length and number of twins, until finally an extremely small grain size results with an absence of twins. Unfortunately, at the swaging temperature at which this fine grain size could be produced, the specimens cracked longitudinally.

At present, work is being done to ascertain at what stage of the swaging process the cracking originates. By learning this, it may then be possible to alter the swaging process so as to produce a fine grain size without longitudinal cracking. At the same time, an effort will be made to follow systematically this apparent dynamic recrystallization at various stages of the swaging operation.

5. ELECTRON TRANSMISSION MICROSCOPY

During the quarter covered by this report, the study of dislocations in foils cut from bulk specimens deformed in tension continued. Particular attention was paid to the examination of foils prepared from the beryllium copper alloys described in another section of this report. The techniques used for cutting, shaping and thinning pure beryllium proved for the most part to be applicable to the beryllium copper alloys. Difficulty was encountered in the final stages of electropolishing. The electrolyte used for pure beryllium, containing 90 parts phosphoric acid, 30 parts sulphuric acid, 30 parts ethanol and 30 parts glycerine, produced a reddish brown film on the specimen at low current densities. Optically bright surfaces were obtained by critically adjusting the current density while observing the surfaces. Examination of the foils in the electron microscope revealed that the surface was considerably rougher than those obtained for pure beryllium and the dislocation

contrasts were frequently obscured. The best polish was obtained by frequently changing the polishing bath.

Preliminary observations were conducted on a beryllium copper single crystal which had been deformed for prism slip. The $\{11\bar{2}0\}$ surface was parallel to the plane of the foil and the [0001] was normal to the tensile axis. The extinction contours were found to lie in bands parallel to the [0001] direction and perpendicular to the growth axis (also tension axis), as shown in Figure 13. This suggested that the surface was corrugated as a result of preferential attack of the surface during electro-polishing. Such segregation of solute during the solidification of crystals grown from the melt are known to occur as a result of constitutional super-cooling or as a result of fluctuations in the growth conditions during zone refining. Additional observations of other alloyed crystals will be required before any conclusions may be drawn about the segregation of copper in beryllium.

The dislocations in Figure 13 for the alloyed crystal have many similarities to the dislocations observed for pure beryllium deformed for prism glide. Dislocations appear to have been impeded at tiny dislocation loops, as reported for pure beryllium. Further studies of the alloy crystals are anticipated. One is interested to compare the dislocations in the alloy crystals with those observed in the pure beryllium crystal. It is important to determine whether the stacking fault energy of the alloyed crystals is lowered sufficiently to reveal extended nodes, pile up of dislocations on the basal plane and the elimination of cross slip from the basal to prism plane.

In addition to this work on foils the examination of slip lines using replicating techniques is anticipated. Preliminary work to develop techniques for replicating slip lines has started. The techniques being tried are due to Bradley[2] and Fourie[3].

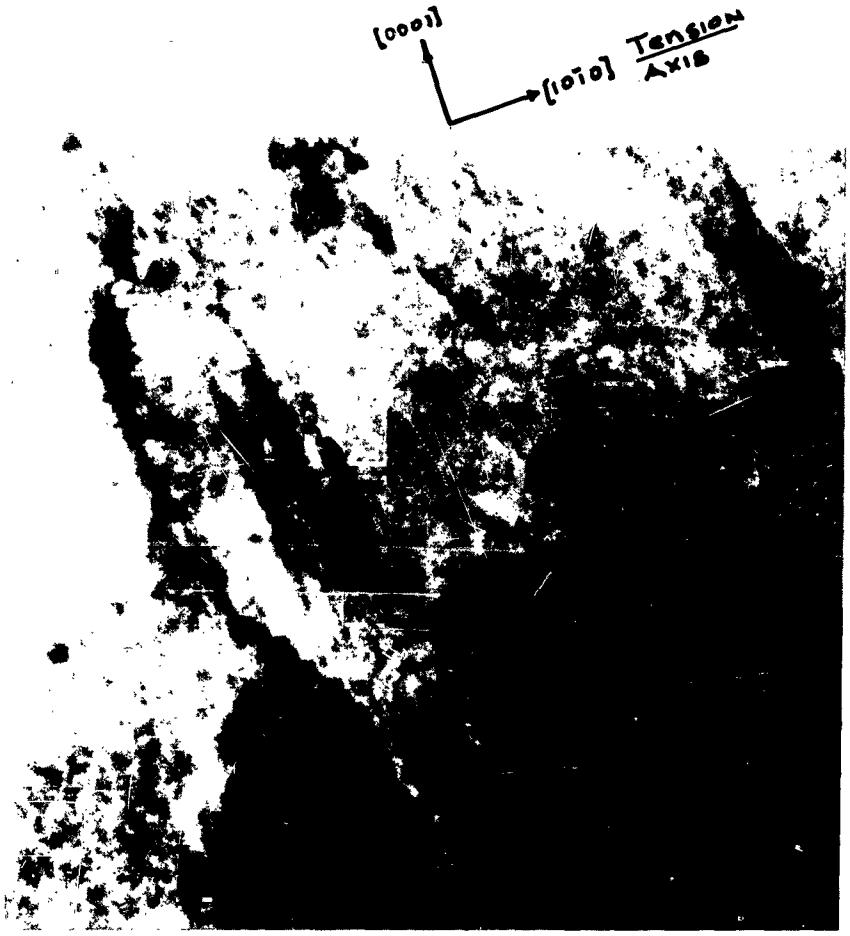

FIG. 13. ELECTRON TRANSMISSION MICROGRAPH OF BeCu ALLOY CRYSTAL DEFORMED FOR PRISM SLIP. MAG. 21,000X

Q-B2089-1

6. SELF-DIFFUSION IN BERYLLIUM

6.1 Self-Absorption of Beryllium γ-Radiation

6.1.1 Introduction

In order to use either the residual activity method or the surface counting method to determine the concentration profile of a radioactive diffusing tracer, a detailed knowledge of the radiation absorption coefficient of the particular diffusion system is necessary. Although measurements of γ-ray absorption coefficients of many combinations of elements have been made in the past, no value of the self-absorption coefficient of the γ-radiation of Be^7 can be found in the literature. It is the purpose of this part of the present investigation to measure the self-absorption coefficient of beryllium γ-radiation. According to the existing theory of γ-ray absorption, a theoretical value for beryllium self-absorption is also calculated.

6.1.2 Review of Previous Investigations

The interaction of γ-rays with matter has been studied very extensively during the past two decades. Theories for different types of γ-ray interaction with matter have been developed. Davisson and Evans[4,5] have made comprehensive investigations of this subject. They measured the absorption of γ-rays in Al, Cu, Sn, Ta and Pb by using the γ-emissions of I^{131}, Cu^{64}, Mn^{54}, Co^{60}, Zn^{65}, and Na^{24}. They have also made a detailed study of the theories of the absorption processes for the γ-rays of energy ranging from 0.1 mev to 6.0 mev. In general, three types of interaction of γ-rays with matter are considered to occur. They are: 1) the photoelectric effect, in which a photon gives all its energy to a bound electron, which uses part of the energy to overcome its binding to the atom and takes the rest as its kinetic energy upon emission; 2) the Compton effect, in which a photon is scattered by an electron of the atom, the photon going off in a different

Q-B2089-1

direction with decreased energy and the electron recoiling with the remaining energy; 3) pair production, in which a photon in the field of the nucleus produces an electron-position pair, whose total energy is equal to the energy of photon.

The three processes act independently of each other. Each of these is responsible for a certain portion of the intensity change occurring when γ-radiation passes through an absorber. Let ΔI_p, ΔI_c and ΔI_e represent the components of the intensity change due to photoelectric, Compton effect and electron-position pair production, respectively, and τ, σ and κ be their corresponding absorption coefficients. The ratio of the intensity change to incident radiation is found to be proportional to the small thickness ΔX of the absorber as:

$$\Delta I_p/I = -\tau \Delta X \qquad (1)$$

$$\Delta I_c/I = -\sigma \Delta X \qquad (2)$$

$$\Delta I_e/I = -\kappa \Delta X \qquad (3)$$

The sum of the fractions may be expressed as

$$\frac{\Delta I}{I_o} = -(\tau + \sigma + \kappa)\Delta X \qquad (4)$$

or

$$\Delta I/I_o = -\mu \Delta X \qquad (5)$$

where μ is defined as total linear absorption coefficient. If μ is a constant, the integration of Equation 5 yields:

$$\frac{I}{I_o} = \exp(-\mu X) \qquad (6)$$

Equation 6 gives the intensity of radiation, I, after a beam of initial intensity, I_o, has transversed the thickness, X, of a particular material. It is the basic equation by which the absorption coefficient μ is experimentally determined.

Q-B2089-1

6.1.3 Experimental Procedure and Results

Radioactive beryllium (Be^7) was obtained from Nuclear Science and Engineering Corporation where it was prepared by cyclotron activation of lithium chloride. The radiochemical purity is estimated as better than 99%, Be^7 has a 0.48 mev γ-emission with a half life of about 53 days and a soft x-ray emission of 52 ev. The source of Be^7 for this measurement was prepared by deposition a small amount of $BeCl_2$ on to the surface of a piece of metal. This thin point source was immediately covered by a piece of transparent scotch tape in order to hold the source on the surface of the metal.

The absorbers were cut from an extruded, SR grade, Pechiney beryllium bar. The density of the beryllium bar was found to be 1.85 gr/cm^3. Wafers of different thickness from 0.02" to 0.25" were prepared with parallel surfaces.

A 2π-geometry scintillation counter was used to measure the radioactivity of the source. A collimator was made of α-brass which also serves as the absorber holder. The source was placed about 6 centimeters away from the counter. The geometry of the counter system is shown in Figure 14.

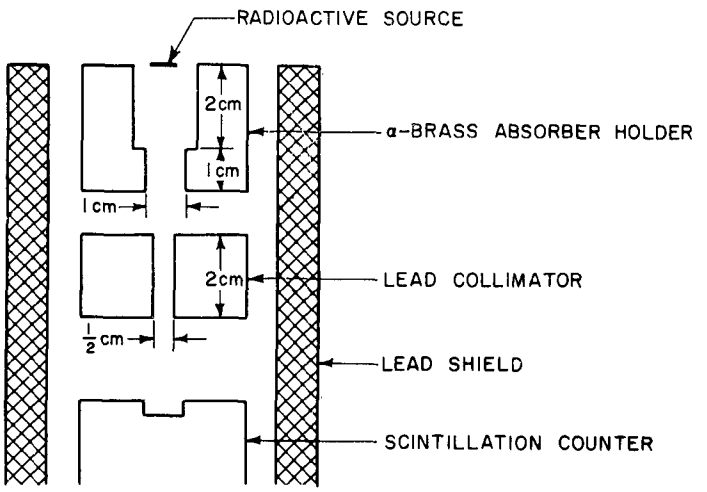

FIG. 14. SCHEMATIC PLAN VIEW OF γ-RADIATION COUNTING APPARATUS

In Figure 15, the logarithim of the radioactivity measured after passing through absorbers was plotted against the thickness of the absorbers. The value of the total linear absorption coefficient, μ determined from the slope of the plot is 0.11 cm^{-1}.

6.1.4 Discussion

As mentioned previously, three mechanisms can participate in the γ-ray absorption process depending on the energy of the γ-emission. Therefore, the absorption coefficients of the three processes are expected to vary with the energy of the emission and the atomic number of the absorber. In order to determine the dominant process in the

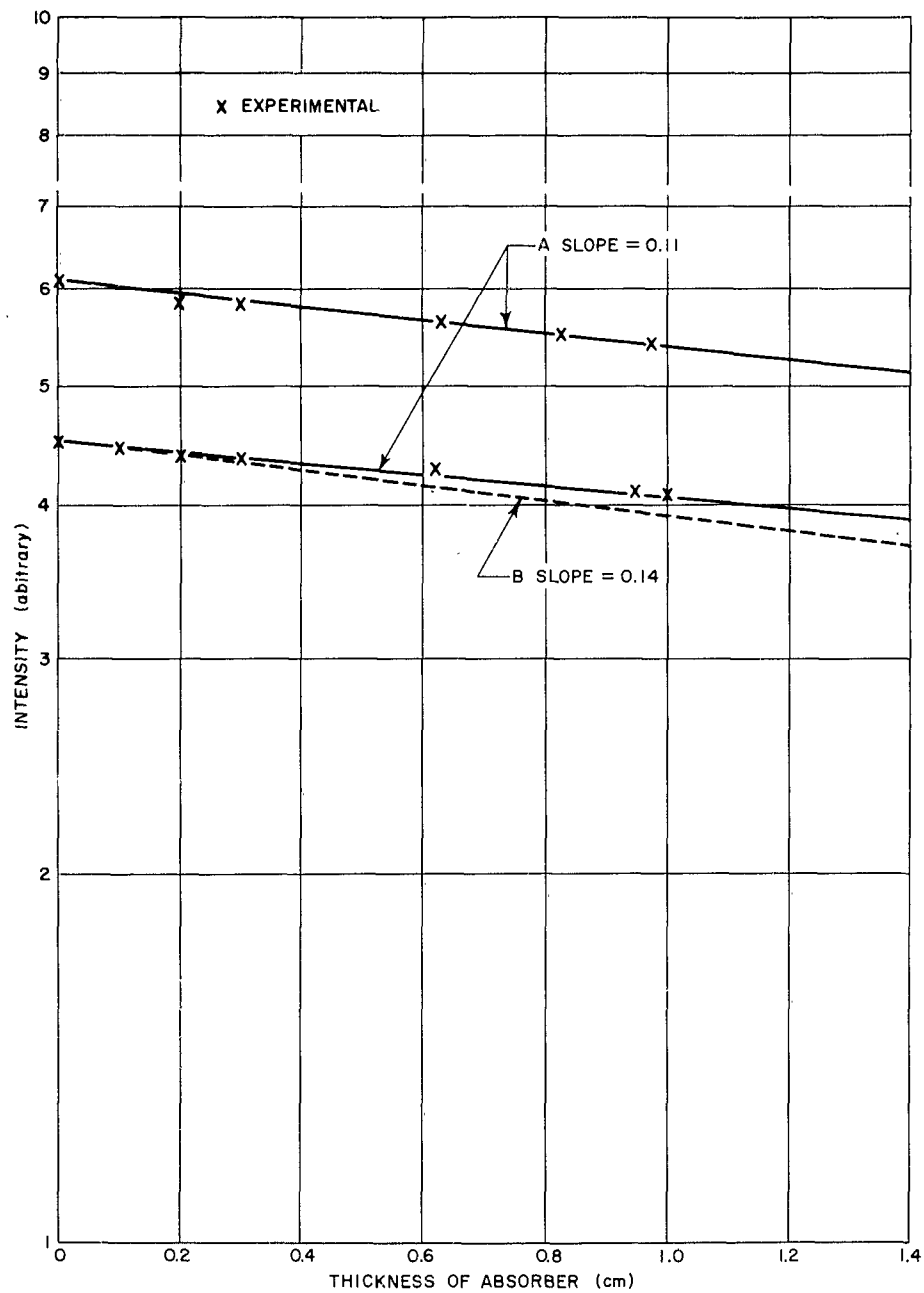

FIG.15. PLOT OF INTENSITY vs. THICKNESS OF ABSORBER IN COMPARISON WITH THEORY

Q-B2089-1

absorption of γ-rays by Be, the measured value of μ will be compared to theoretical estimates of the contributions due to each process.

It is known that the rest mass energy of an electron-position pair is about 1.02 mev. In order to produce such a pair of particles, each photon of the γ-radiation must give up 1.02 mev of its energy or more during its interaction with the absorber. Since the γ-emission of Be^7 has a kinetic energy of about 0.48 mev, the pair production process should not appear in the self-absorption system of beryllium.

Hulme, McDougall, Buckingham and Fowler[6] have carried out an exact calculation of the photoelectric absorption coefficient for the energy range from 0.35 mev to 2 mev and the atomic number of the absorber ranging from 0 to 38. According to their calculations, the photoelectric self-absorption coefficient of beryllium can be evaluated as:

$$\tau = 2.5 \times 10^{-32} \quad \frac{\rho n \quad NZ^5}{A} \qquad (7)$$

where ρ is the density of the beryllium absorber; η, the energy ratio of a photoelectron of the rest mass of the γ-radiation; N, Avogadro's number, Z, the atomic number, and A, the atomic weight of beryllium. τ is calculated as 3.2×10^{-6} cm^{-1}, which is negligibly small in comparison with the experimental total absorption coefficient.

After eliminating the pair production and the photoelectron effect mechanisms for the particular absorption system, the dominating cause of the absorption must be the Compton effect.

Klein and Nishina[7] have carried out a quantum mechanical treatment on the subject of γ-ray energy scattering. In a given direction, they have obtained the equation

$$I = I_o \quad \frac{e^4}{2\, m^2 c^4 r^2} \; \frac{1 + \cos^2 \theta}{[1 + \alpha\,(1-\cos\theta)]^3} \left\{ 1 + \frac{\alpha^2\,(1 - \cos\theta)^2}{1+\cos^2\theta)\;[1+\alpha\,(1-\cos\theta)]} \right\} \qquad (8)$$

Q-B2089-1

where I_o is the intensity of the incident beam γ-ray; I, the intensity of the scattered beam at the angle θ; r, the distance from the scattering electron of charge, e and mass, m, and $\alpha = h\nu/mc^2$, the energy ratio. [illegible][8] and Davisson and Evans[5] have derived [illegible] equation for the calculation of the total cross section of the absorption coefficient σ due to the Compton effect. Using linear dimensions, the equation can be expressed as:

$$\sigma = 2\pi r_o^2 \left\{ \frac{1+\alpha}{\alpha^2} \left[\frac{2(1+\alpha)}{1+2\alpha} - \frac{1}{\alpha} \ln (1+2\alpha) \right] + \frac{1}{2\alpha} \ln (1+2\alpha) - \frac{1+3\alpha}{(1+2\alpha)^2} \right\} \quad (9)$$

Where $r_o = e^2/mc^2$ is a constant which has a value of about 1.99×10^{-13}; ρ, N, Z and A are as defined in Equation 7, and $\alpha = h\nu/mc^2$ is the energy ratio. Carrying out the calculation for beryllium self-absorption, one obtains a value for μ which is 0.14 cm^{-1}.

The "best" straight line drawn through the experimental points as shown in Figure 15 gives a value of μ equal to .11 cm^{-1}. Line B corresponds to the theoretical value (.14 cm), calculated above. The causes of the deviation at large values of X are currently being investigated.

Marvin Herman, Manager
Metallurgical Laboratory

Approved by

H. G. F. Wilsdorf
Technical Director

Q-B2089-1

REFERENCES

1. G. E. Spangler, et al, Franklin Institute Quarterly Progress Report, Q-B1933-5, January 1, 1963.

2. D. E. Bradley, Inst. Metals, 83, 1561, (1954-55).

3. J. T. Fourie, Appl. Phys. 29, 608 (1958).

4. C. M. Davisson and R. D. Evans, Phys. Rev. 81, 404 (1951).

5. C. M. Davisson and R. D. Evans, Review of Modern Physics, 24, 79 (1952).

6. Hulme, McDougall, Buckingham and Fowler, Proc. Roy. Soc. (London) 149A, 131 (1935).

7. O. Klein and Y. Nishina, Z. Physik, 52, 853 (1929).

8. W. Heitler, The Quantum Theory of Radiation, Oxford University Press, London, 1944, p. 159.

Q-B2089-1

DISTRIBUTION LIST

Department of the Navy
Bureau of Naval Weapons
Washington 25, D. C.
Attn: RRMA-222

Brush Beryllium Company
4303 Perkins Avenue
Cleveland 3, Ohio
Attn: Mr. W. W. Beaver

Battelle Memorial Institute
505 King Avenue
Defense Metals Information Center
Columbus 1, Ohio

Lockheed Aircraft Corporation
Lockheed Missile Systems Div.
Hanover Street
Palo Alto, California
Attn: Dr. John C. McDonald

Department of the Army
Chief of Ordnance
Washington 25, D. C.
Attn: ORDTB-Materials

The Alloyd Corporation
35 Cambridge Parkway
Cambridge 42, Mass.
Attn: Dr. L. McD. Schetky

Commander
Ordnance Corps. Frankford Arsenal
Pitman Dunn Laboratory
Phila. 37, Pa.
Attn: Mr. D. Kleppinger

Director, U. S. Naval Research Lab.
Metallurgy Division
Washington 25, D. C.
Attn: Mr. W. Pellini

Commander
Aeronautical Systems Division
Wright-Patterson Air Force Base, Ohio
Attn: ASRCMP-1

Nuclear Metals, Inc.
Concord, Massachusetts
Attn: Dr. A. Kaufmann

University of California
Lawrence Radiation Laboratory
P. O. Box 808
Livermore, California
Attn: Mr. Clovis G. Craig
Technical Information

The Beryllium Corporation
P. O. Box 1462
Reading, Pa.
Attn: Mr. William Santschi

Avco Manufacturing Corporation
Research and Advanced Dev. Div.
201 Lowell Street
Wilmington, Massachusetts
Attn: Dr. S. R. Maloff

Commander
Watertown Arsenal
Watertown 72, Massachusetts
Attn: Mr. S. Arnold

Chief of Naval Research (ORN:423)
Department of the Navy
Washington 25, D. C.

U. S. Atomic Energy Commission
Division of Reactor Development
Engineering Development Branch
Washington 25, D. C.
Attn: Mr. J. M. Simmons
Chief, Metallurgy Section

Q-B2089-1

DISTRIBUTION LIST (cont.)

The Rand Corporation
Aeronautics Department
1700 Main Street
Santa Monica, California
Attn: George Hoffman

Stauffer-Temescal Company
1201 South 47th Street
Richmond, California
Attn: Dr. Charles Hunt

Boeing Airplane Company
Seattle Division
Seattle, Washington
Attn: Mr. George Hughes

F. A. Crossley
Research Metallurgist
Metals Research Department
Armour Research Foundation
Chicago 16, Illinois

U. S. Atomic Energy Commission
Technical Information Service
P. O. Box 62
Oak Ridge, Tennessee

National Aeronautics and Space Adm.
1520 H Street, N. W.
Washington, D. C. (3)

Raytheon Manufacturing Co.
Waltham 54, Massachusetts
Attn: Mr. J. F. Ahern

Westinghouse Electric Cor.
Air Arm. Division
Materials & Process Section 478
P. O. Box 746
Baltimore 3, Md.
Attn: Mr. A. T. Hamill, Manager

Department of the Navy
Bureau of Ships
Washington 25, D. C.
Attn: Code 345

Oak Ridge National Laboratory
P. O. Box X
Oak Ridge, Tennessee
Attn: Mr. W. D. Manly

Republic Aviation Corporation
Farmingdale, Long Island, New York
Attn: Mr. Harry A. Pearl, Chief,
Materials Development Div.

Sperry Gyroscope Company
Division of Sperry Rand
Great Neck, New York
Attn: Mr. R. H. Schoemann
Senior Materials Engineer

Commander
Naval Air Material Center
Aeronautical Materials Lab.
Philadelphia Naval Base
Phila. 12, Pa.

Westinghouse Electric Co.
Electronics Division
P. O. Box 1897
Baltimore 3, Maryland

Thompson-Ramo Wooldridge, Inc.
Cleveland, Ohio
Attn: Mr. Lazer

Bell Telephone Laboratories
Whippany, New Jersey
Attn: Mr. A. H. Fitch,
Code 3B-356

Southern Research Institute
2000 Ninth Avenue S.
Birmingham 5, Alabama
Attn: Mr. J. Morrison

DISTRIBUTION LIST (cont.)

National Academy of Sciences
Materials Advisory Board
2101 Constitution Avenue
Washington 25, D. C.
Attn: Dr. Joseph Lane

Mr. R. L. Keane
Resident Representative
c/o University of Penna.
3438 Walnut Street
Phila. 4, Pa.

Mr. Lewis Rogers
Vitro Laboratories
West Orange Laboratory
200 Pleasant Valley Way
West Orange, New Jersey

Northrop Corporation
Norair Division
Hawthorne, California
Dept. 3552, Zone 32
Attn: L. M. Christensen
Via: Bureau of Naval Weapons Rep
Inglewood, California

General Astrometals Corporation
320 Yonkers Avenue
Yonkers, New York
Attn: W. Lidman, Technical Director

Dr. R. F. Bunshah
University of California
Lawrence Radiation Laboratory
P. O. Box 808
Livermore, California

Radiation Application Inc.
36-40 37th Street
Long Island City 1, N. Y.

U. S. Atomic Energy Commission
Technical Services Division
New York Operations Office
376 Hudson Street
New York 14, N. Y.

Curtiss Wright Corporation
Wright Air Development Division
Wood-Ridge, New Jersey
Attn: Mr. Henry Hahn

Dr. Thomas J. Hughel
Metallurgical Engineering Dept.
Research Laboratories
General Motors Corp.
12 Mile and Mound Roads
Warren, Michigan

Commander
Armed Services Technical Info., Agency
Arlington Hall Station
Arlington 12, Virginia (10)

Aerojet-General Corporation
P. O. Box 296
Azisa, California
Attn: Dr. Preston L. Hiel
Technical Specialist
Structural Materials Div.
Department 322

VIA: H. G. F. Wilsdorf
Metallurgy (B. Thompson)
Central File